Inorganic Chemistry

pubs.acs.org/IC

Featured Article

Catalytic H_2O_2 Activation by a Diiron Complex for Methanol Oxidation

Thomas Philipp Zimmermann,[†] Nicole Orth,[†] Sebastian Finke, Thomas Limpke, Anja Stammler, Hartmut Bögge, Stephan Walleck, Ivana Ivanović-Burmazović,* and Thorsten Glaser*

Cite This: https://dx.doi.org/10.1021/acs.inorgchem.0c02698

Read Online

ACCESS | Metrics & More | Article Recommendations | Supporting Information

ABSTRACT: In nature, C−H bond oxidation of CH_4 involves a peroxo intermediate that decays to the high-valent active species of either a "closed" $\{Fe^{IV}(\mu\text{-}O)_2Fe^{IV}\}$ core or an "open" $\{Fe^{IV}(O)(\mu\text{-}O)Fe^{IV}(O)\}$ core. To mimic and to obtain more mechanistic insight in this reaction mode, we have investigated the reactivity of the bioinspired diiron complex $[(susan)\{Fe(OH)(\mu\text{-}O)Fe(OH)\}]^{2+}$ [susan = 4,7-dimethyl-1,1,10,10-tetrakis(2-pyridylmethyl)-1,4,7,10-tetraazadecane], which catalyzes CH_3OH oxidation with H_2O_2 to HCHO and HCO_2H. The kinetics is faster in the presence of a proton. ^{18}O-labeling experiments show that the active species, generated by a decay of the initially formed peroxo intermediate $[(susan)\{Fe^{III}(\mu\text{-}O)(\mu\text{-}O_2)Fe^{III}\}]^{2+}$, contains one reactive oxygen atom from the μ-oxo and another from the μ-peroxo bridge of its peroxo precursor. Considering an $Fe^{IV}Fe^{IV}$ active species, a "closed" $\{Fe^{IV}(\mu\text{-}O)_2Fe^{IV}\}$ core explains the observed labeling results, while a scrambling of the terminal and bridging oxo ligands is required to account for an "open" $\{Fe^{IV}(O)(\mu\text{-}O)Fe^{IV}(O)\}$ core.

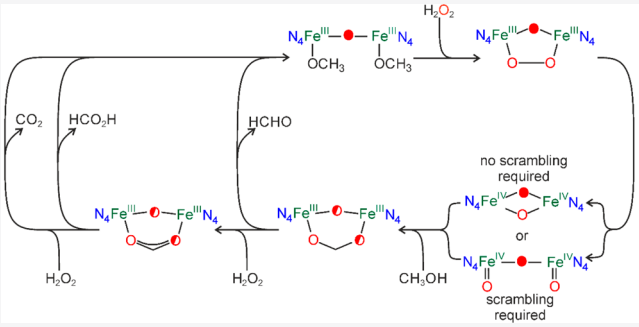

■ INTRODUCTION

Nonheme diiron enzymes activate dioxygen (O_2) in biological systems to catalyze various oxidation and/or oxygenation reactions.[1−3] Examples are soluble methane monooxygenase (sMMO), which selectively catalyzes the two-electron oxidation of methane (CH_4) to methanol (CH_3OH),[4−6] or arylamine *N*-oxygenase (CmlI), which catalyzes the six-electron oxidation of aminoarenes to nitroarenes in three two-electron steps.[7,8] The generalized catalytic cycle employs a diferrous form that reacts with O_2 to a peroxo diferric intermediate.[1] The active species is proposed to be either this peroxo intermediate or a high-valent species resulting from its conversion. In sMMO, the active species is thought to be a high-valent $Fe^{IV}Fe^{IV}$ intermediate termed **Q**,[1,4−6] with a "closed" $\{Fe^{IV}(\mu\text{-}O)_2Fe^{IV}\}$ core[9,10] or, more recently proposed, an "open" $\{Fe^{IV}(O)(\mu\text{-}O)Fe^{IV}(O)\}$ core[11,12] structure. After substrate oxidation, the active site is in a diferric form, which must be reduced by two electrons to retrieve the starting diferrous form. However, the diferric form can also react with hydrogen peroxide (H_2O_2) to form the peroxo intermediate (peroxide shunt).[13,14]

Besides the structural characterization of diiron model complexes with a μ-1,2-peroxo bridge,[15−18] important mechanistic insights were obtained by studying the reactions of diferric complexes of tris(2-pyridylmethyl)amine (tpa)-based ligands with H_2O_2. These studies have provided strong differences in the stabilities and reactivities of the peroxo complexes induced by slight variations of the tpa-based ligand substituents. In some instances, a transient $\{Fe^{III}(\mu\text{-}O)(\mu\text{-}O_2)Fe^{III}\}$ intermediate could be observed by its characteristic absorption features around 15500 and 20000 cm^{-1} assigned to μ-peroxo → Fe^{III} and μ-oxo → Fe^{III} ligand-to-meatl charge transfers, respectively.[19−22] Also, a $\{Fe^{III}(\mu\text{-}OH)(\mu\text{-}O_2)Fe^{III}\}$ transient intermediate with a broad maximum of around 14300 cm^{-1} was postulated.[23] However, the peroxo intermediates were not observable in the majority of cases even at low temperatures because of their high reactivity. Instead, their decay with the formation of high-valent $Fe^{IV}Fe^{III}$[23−25] or $Fe^{IV}Fe^{IV}$[26−31] species could be established.

To mimic the reactivity of oxygenating enzymes and to develop bioinspired homogeneous catalysts, we synthesized a dinucleating ligand system consisting of two ethylene-bridged tripodal ligand compartments with varying terminal donors,[32−34] e.g., the ligand 4,7-dimethyl-1,1,10,10-tetrakis(2-pyridylmethyl)-1,4,7,10-tetraazadecane (susan; Figure 1a). Here, we present a detailed study on the reactivity of diferric complexes of susan toward H_2O_2 in CH_3OH. We observed a

Received: September 9, 2020

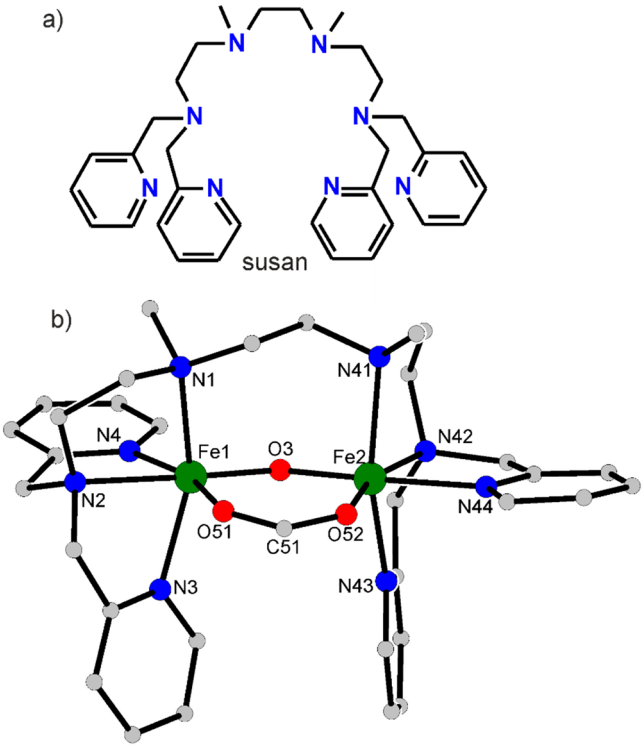

Figure 1. Structural presentations of the ligand and complex: (a) the ligand susan; (b) molecular structure of $\mathbf{1}^{3+}$ in single crystals of $[(susan)\{Fe(\mu\text{-}O)(\mu\text{-}O_2CH)Fe\}](ClO_4)_3\cdot{}^1/_2MTBE$. Hydrogen atoms have been omitted for clarity. Selected bond lengths: Fe1−O3 1.785(6), Fe1−O51 2.075(8), Fe1−N1 2.199(9), Fe1−N2 2.225(10), Fe1−N3 2.133(9), Fe1−N4 2.131(8), Fe2−O3 1.800(6), Fe2−O52 1.990(10), Fe2−N41 2.266(11), Fe2−N42 2.176(10), Fe2−N43 2.140(10), Fe2−N44 2.200(10), Fe1···Fe2 3.288(2).

catalytic oxidation of CH_3OH to formaldehyde (HCHO) and formic acid (HCO_2H). A peroxo intermediate was formed, which then converted to an even more reactive high-valent species. The role of protonation of the coordinated peroxide was investigated, and isotope-labeling studies provided important mechanistic insight.

■ RESULTS AND DISCUSSION

Reactivity and Catalytic Studies. The reaction of susan with 2 equiv of $Fe(ClO_4)_2\cdot6H_2O$ and an excess of H_2O_2 in CH_3OH resulted in a bubble release and a temperature increase. Diffusion of methyl *tert*-butyl ether (MTBE) yielded single crystals of the formato-bridged complex $[(susan)\{Fe(\mu\text{-}O)(\mu\text{-}O_2CH)Fe\}](ClO_4)_3\cdot0.5MTBE$ [$\mathbf{1}(ClO_4)_3\cdot0.5MTBE$; Figure 1b]. The closely related acetato-bridged complex $[(susan)\{Fe(\mu\text{-}O)(\mu\text{-}OAc)Fe\}](ClO_4)_3$ [$\mathbf{2}(ClO_4)_3$] was synthesized in a straightforward reaction of susan with 2 equiv of $Fe(ClO_4)_2\cdot6H_2O$ and 1 equiv of $(Bu_4N)OAc$ under basic conditions in an ethanol/acetone mixture, i.e., without the addition of H_2O_2.[35]

The unexpected presence of formate in $\mathbf{1}^{3+}$, without providing its source, raises a question of its origin. Que and co-workers obtained a μ-oxo-μ-formato-bridged diferric complex in the reaction of tpa with $Fe^{III}(ClO_4)_3\cdot10H_2O$ and triethylamine in CH_3OH.[36] They assigned the origin of the formato bridge to the oxidation of coordinated CH_3OH by O_2. In order to exclude impurities as a formate source, we performed the reaction with more concentrated solutions and obtained reproducible yields of 71%, which would require 9.8 mM concentrations of formate. Gas chromatography−mass spectrometry (GC−MS) analysis ruled out contaminations in this order of magnitude [see the Supporting Information (SI) for details]. Moreover, without the addition of H_2O_2, there is no indication for the formation of $\mathbf{1}^{3+}$, and in the absence of the iron species, no significant formate concentrations could be detected by the reaction of CH_3OH and H_2O_2, under analogous conditions even after 3 days. Thus, a dinuclear susan complex is required to activate an excess of H_2O_2 toward the in situ four-electron oxidation of CH_3OH to formate in two two-electron steps, as demonstrated by various labeling experiments utilizing $H_2{}^{18}O_2$ and $H_2{}^{18}O$ (vide infra).

To investigate this reactivity in more detail, we employed $[(susan)\{Fe(OH)(\mu\text{-}O)Fe(OH)\}](ClO_4)_2$ [$\mathbf{3}(ClO_4)_2$][37] with terminal OH^- ligands as a well-defined precursor. In a CH_3OH solution, $\mathbf{3}(ClO_4)_2$ undergoes solvolysis to $[(susan)\{Fe(OMe)(\mu\text{-}O)Fe(OMe)\}]^{2+}$ ($\mathbf{4}^{2+}$) even at −80 °C (see the SI for details). We reacted $\mathbf{4}^{2+}$ in CH_3OH with 1360 equiv of H_2O_2 at room temperature and quenched the reaction after 30 min by the addition of aqueous hydrochloric acid. Through extraction with trichloromethane ($CHCl_3$; or $CDCl_3$), we identified two reaction products in the organic phase by independent GC−MS and NMR analysis: the methyl ester of formic acid (HCO_2CH_3; a four-electron oxidation product) and the dimethyl acetal of formaldehyde [$H_2C(OCH_3)_2$; a two-electron oxidation product]. Quantitative analysis (see the SI for details) provided turnover numbers of 74(5) and 62(5) for HCO_2CH_3 and $H_2C(OCH_3)_2$, respectively. It should be noted that these numbers constitute only lower limits as gaseous products were detected: on the one hand, O_2, which is indicative of catalase activity,[38,39] and, on the other hand, CO_2, which is indicative of six-electron oxidation of CH_3OH. These gaseous products could facilitate the loss of other volatile oxidation products into the gaseous phase.

To obtain more insight into the second two-electron oxidation from HCHO to HCO_2H, we performed the same reaction but preadded 74 equiv of HCHO, yielding 127(15) and 78(11) equiv of $H_2C(OCH_3)_2$ and HCO_2CH_3, respectively. It should be considered that under these conditions also the oxidation of CH_3OH contributes to these yields (vide supra). A comparison of the observed yields indicates that $\mathbf{3}^{2+}$ does not significantly utilize free HCHO as a substrate for the oxidation by H_2O_2 to HCO_2H.

These experiments indicate that (i) H_2O_2 is activated by a susan diiron species, which is (ii) capable of oxidizing CH_3OH by two electrons to a HCHO derivative but (iii) not active toward the oxidation of free HCHO; thus, (iv) the second two-electron oxidation most likely occurs, while HCHO is still coordinated.

Mechanistic Studies. The reaction of $\mathbf{4}^{2+}$ in CH_3OH with H_2O_2 was followed by UV−vis−near-IR (NIR) spectroscopy (Figure 2). The addition of 100 equiv of H_2O_2 at room temperature generated a new species (∼20 s, red in Figure 2a) with increased intensity around 17000 cm^{-1}. The difference spectrum after and before H_2O_2 addition (magenta in Figure 2a) reveals two absorption maxima at 16000 and 19300 cm^{-1}, which match the two characteristic absorption bands of μ-1,2-peroxo-μ-oxo-bridged diferric complexes of Que et al. and Kodera et al. with related ligand environments (vide infra),[19,22] indicating formation of the peroxo-bridged complex $[(susan)\{Fe^{III}(\mu\text{-}O)(\mu\text{-}O_2)Fe^{III}\}]^{2+}$ ($\mathbf{5}^{2+}$; Figure 3, top pathway).

https://dx.doi.org/10.1021/acs.inorgchem.0c02698
Inorg. Chem. XXXX, XXX, XXX−XXX

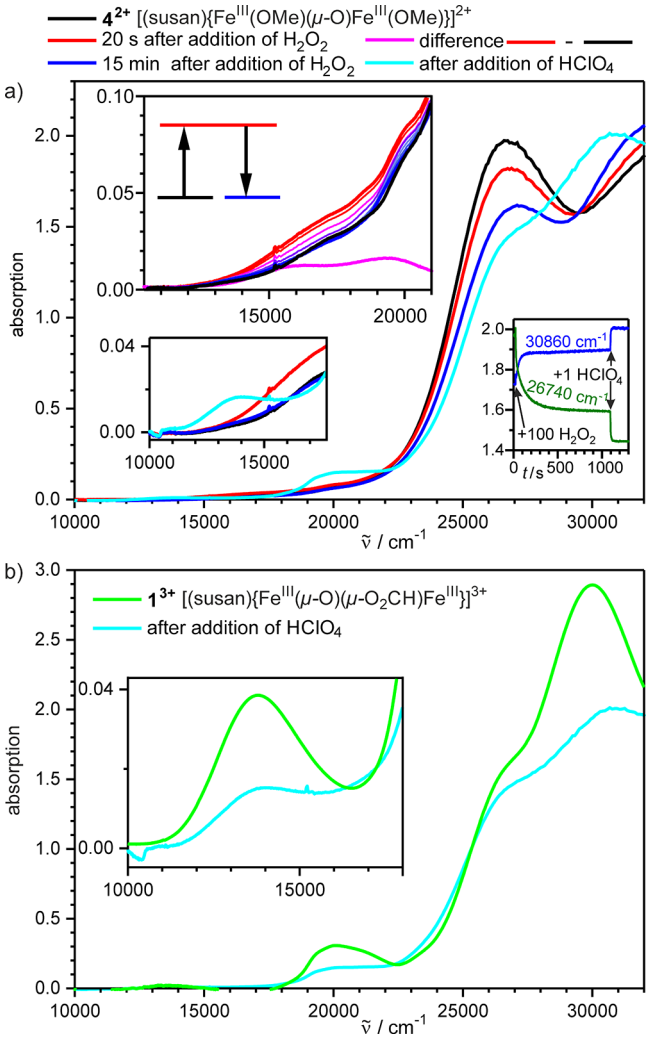

Figure 2. Spectroscopic observation of the reactions with H_2O_2: (a) UV−vis−NIR spectra and time traces at selected wavenumbers for the reaction of $\mathbf{3}(ClO_4)_2$ (0.28 mM) in CH_3OH with 100 equiv of H_2O_2, followed by the addition of 1 equiv of $HClO_4$ at room temperature. The sequence of the addition is indicated in the time traces inset. (b) Comparison of the final spectrum after the addition of $HClO_4$ to the spectrum of $[(susan)\{Fe(\mu\text{-}O)(\mu\text{-}O_2CH)Fe\}]^{3+}$ (for a better comparison, the absorption is corrected to a concentration of 0.28 mM).

$\mathbf{5}^{2+}$ decays exponentially on a slower time scale (∼1000 s) than its formation, as is evident by the decrease of the peroxo bands and the band around 27000 cm^{-1} (inset in Figure 2a).

The resulting species (blue in Figure 2a) comprises the same spectral features as $\mathbf{4}^{2+}$, indicating again a μ-oxo-bridged $[(susan)\{Fe^{III}X(\mu\text{-}O)Fe^{III}X\}]^{2+}$ entity. The addition of 1 equiv of $HClO_4$ results in new absorptions at 14000, 20180, and 30800 cm^{-1} (cyan in Figure 2a) that are the signature of doubly bridged complexes $[(susan)\{Fe^{III}(\mu\text{-}O)(\mu\text{-}O_2CR)\text{-}Fe^{III}\}]^{3+}$.[40] A comparison with $\mathbf{1}^{3+}$ (green in Figure 2b) strongly argues for formation of the μ-formato species $\mathbf{1}^{3+}$ upon the addition of $HClO_4$. This reactivity initiated by acid addition can be assigned to the protonation and dissociation of a terminal anionic donor X^- (here X^- = MeO^- or HCO_2^-), followed by a carboxylate shift from the terminal to bridging coordination mode (Figure 3, top pathway). In the case of acetato complexes, we have shown that this carboxylate shift from $[(susan)\{Fe^{III}(OAc)(\mu\text{-}O)Fe^{III}(OAc)\}]^{2+}$ to $[(susan)\text{-}\{Fe^{III}(\mu\text{-}O)(\mu\text{-}OAc)Fe^{III}\}]^{3+}$ is reversible upon consecutive additions of acid and base.[35] From these data, it can be concluded that either the peroxo intermediate $\mathbf{5}^{2+}$ or a converted high-valent species **Y** initiates the oxidation of CH_3OH with the formation of a μ-oxo-bridged complex possessing a terminal formato ligand that undergoes a carboxylate shift upon the addition of H^+ (Figure 3, top pathway). Note that this reactivity is not observed upon the addition of H^+ only.

The addition of 100 equiv of H_2O_2 at lower temperatures (−40 °C) caused only minor spectral changes over an hour. This is in line with the observed kinetic inertness of $\mathbf{3}^{2+}$ toward ligand exchange, where water exchange on the hydroxido $\mathbf{3}^{2+}$ complex and its monoprotonated (μ-O_2H_3)-bridge form was too slow to be measured.[37] In contrast, double protonation led to the formation of two terminal aqua ligands, which shows increased kinetic lability with a water exchange rate of k_{ex}^{298} = $(3.9 \pm 0.2) \times 10^5$ s^{-1}.

A further influence of protonation on the oxidation reactivity is shown by its dependence on the sequence of addition of H_2O_2 and $HClO_4$ (the data at −50 °C are shown as an example in Figure 4). Monoprotonation resulted in a small shift on a second time scale of the shoulder around 17700 cm^{-1} (Figure 4a) analogous to monoprotonation of $\mathbf{3}^{2+}$ in H_2O.[37] Accordingly, this shift is assigned to protonation of a terminal methoxido ligand (Figure 3, bottom pathway). The subsequent addition of 2 equiv of H_2O_2 initiated intensity increases in the spectrum of around 14000 and 20000 cm^{-1} (blue in Figure 4a). The difference spectrum, 60 min after and before the addition of H_2O_2, indicates the formation of formato-bridged $\mathbf{1}^{3+}$, effected by the addition of H_2O_2 (green in Figure 4a) to the monoprotonated form of $\mathbf{4}^{2+}$ (Figure 3, bottom pathway).

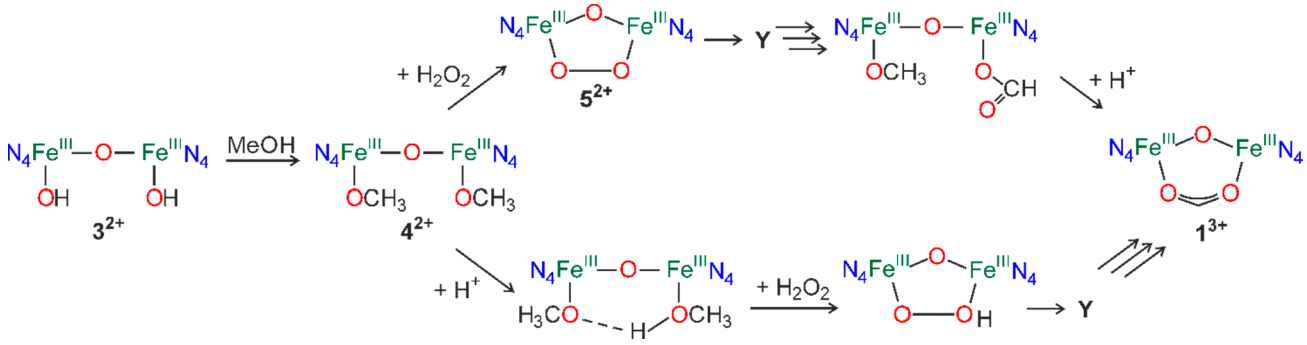

Figure 3. Proton dependence of the reactivity: Different reaction pathways depending on the sequence of addition of oxidant and protons.

https://dx.doi.org/10.1021/acs.inorgchem.0c02698
Inorg. Chem. XXXX, XXX, XXX−XXX

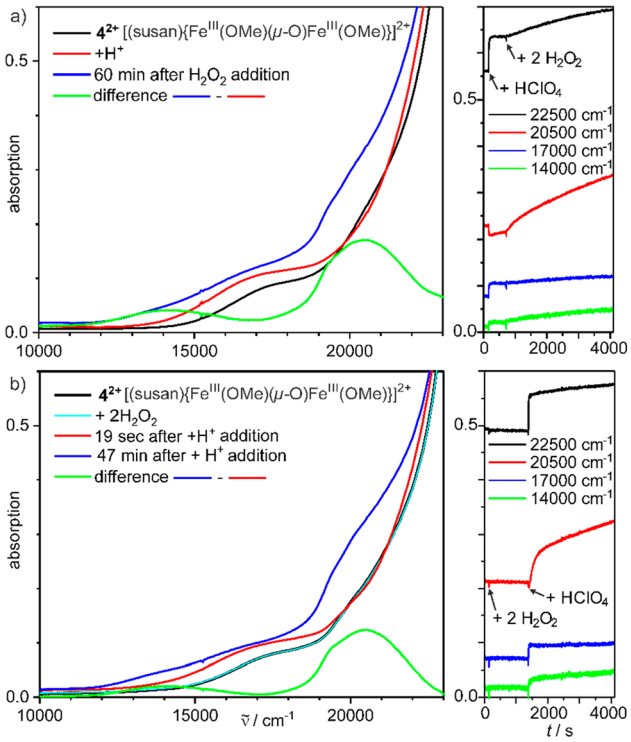

Figure 4. (a) UV−vis−NIR spectra of a 0.73 mM solution of $3(ClO_4)_2$ in CH_3OH at −50 °C and after the consecutive addition of 1 equiv of $HClO_4$ and 2 equiv of H_2O_2. (b) UV−vis−NIR spectra of a 0.65 mM solution of $3(ClO_4)_2$ in CH_3OH at −50 °C and after the consecutive addition of 2 equiv of H_2O_2 and 1 equiv of $HClO_4$. Right: time traces at selected wavenumbers indicating the times of $HClO_4$ and H_2O_2 additions.

In contrast, the addition of 2 equiv of H_2O_2 initially caused no reactivity (black and cyan in Figure 4b), in line with the significantly slower exchange of coordinated OCH_3^- versus CH_3OH at −50 °C. The subsequent addition of one proton equivalent resulted in changes indicative for two reactions (Figure 4b, right). A fast reaction, completed in seconds, consistent with monoprotonation of $\mathbf{4}^{2+}$ (red in Figure 4b) and a slower reaction associated with an intensity increase of around 14000 at 20000 cm^{-1}. The difference spectrum, 47 min and 19 s after $HClO_4$ addition (green in Figure 4b), indicates that the slow reaction is again correlated with the formation of μ-formato-bridged $\mathbf{1}^{3+}$.

These differences demonstrate that protonation of $\mathbf{4}^{2+}$ accelerates the reaction with H_2O_2 to a transient peroxo species. Neither the transient peroxo species nor the converted species can be detected under these conditions but only the final product $\mathbf{1}^{3+}$. This implies the formation of an intermediate more reactive than $\mathbf{5}^{2+}$ in the presence of a proton, presumably a hydroperoxo species.[26,28,41]

To obtain more information, we investigated this reaction by ultrahigh-resolution cold-spray-ionization mass spectrometry (CSI-MS) in CH_3OH at −80 °C. $3(ClO_4)_2$ dissolved in CH_3OH provides solvolyzed $\mathbf{4}^{2+}$ (Figure S2). Upon the addition of 100 equiv of H_2O_2, besides $\mathbf{4}^{2+}$ at m/z 364.1276 as the major peak (Figure S14), a new signal at m/z 349.1047 for the peroxo complex $\mathbf{5}^{2+}$ was detected. A signal at m/z 371.1166 corresponding to $[(susan)\{Fe(O_2CH)(\mu\text{-}O)Fe(OMe)\}]^{2+}$ indicates that some oxidation of CH_3OH to formate occurs already at −80 °C. The addition of 1 equiv of $HClO_4$ significantly changed the MS spectrum (Figure S15). The final product $\mathbf{1}^{3+}$ (m/z 237.0724) and $\{\mathbf{1}(ClO_4)\}^{2+}$ (m/z 405.0822) appeared as the main peaks. Furthermore, a species at m/z 378.1067 corresponding to $([(susan)\{Fe(O_2CH)(\mu\text{-}O)Fe(O_2CH)\}]^{2+}$ was observed. The signal at m/z 349.1034 for the peroxo complex $\mathbf{5}^{2+}$ was of decreased intensity. Warming the reaction to −10 °C slightly changed the ratios of the signals. The peroxo species $\mathbf{5}^{2+}$ was still detected. This

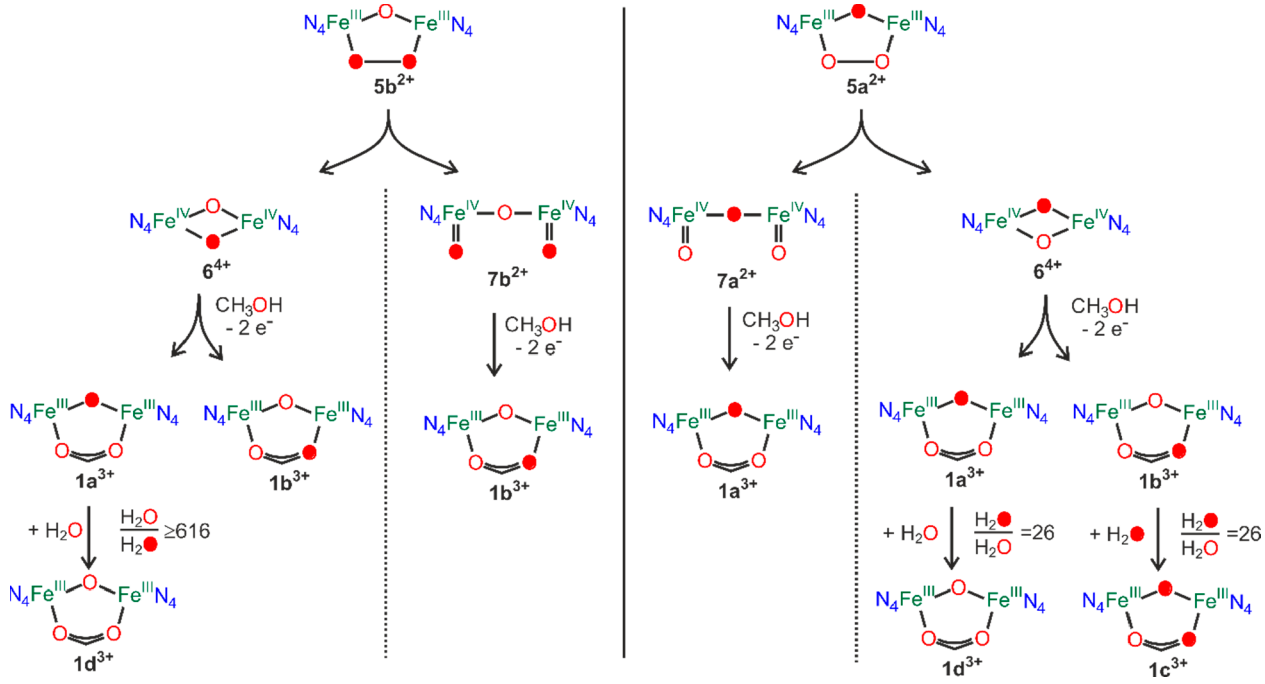

Figure 5. Different reaction pathways in the ^{18}O-labeling experiments, with $H_2{}^{18}O_2$ (left) and $H_2{}^{18}O$ (right) considering "open" and "closed" core oxidants.

https://dx.doi.org/10.1021/acs.inorgchem.0c02698
Inorg. Chem. XXXX, XXX, XXX−XXX

temperature stability of $\mathbf{5}^{2+}$ suggests that it is not the oxidizing species itself but rather a precursor to a transient high-valent species **Y**, which is too reactive to be detected even at −80 °C. On the other hand, protonation of $\mathbf{4}^{2+}$ strongly accelerates the ligand exchange with H_2O_2, presumable forming a hydroperoxo species,[26,28,41] which on a fast time scale generates the active oxidant **Y** and the formato-bridged $\mathbf{1}^{3+}$.

Isotope-Labeling Studies. To further substantiate the proposed reaction scheme, we performed isotopic labeling experiments. Performing the reaction in $^{13}CH_3OH$ shifted the main signal in CSI-MS for $\mathbf{4}^{2+}$ from m/z 364.1275 to 365.1311, proving the incorporation of two $^{13}CH_3O^-$ ligands from the solvent (Figure S16). The addition of 100 equiv of H_2O_2 resulted in the formato species $[(susan)\{Fe(O^{13}CH_3)(\mu\text{-}O)Fe(O_2{}^{13}CH)\}]^{2+}$ at m/z 372.1212 as the main species (Figure S17), and the addition of $HClO_4$ provided $\{\mathbf{1}(ClO_4)\}^{2+}$ as the main species but shifted due to ^{13}C incorporation (m/z 405.5843 in Figure S18). The only unshifted signal is m/z 349.1038, proving its assignment to the peroxo complex $\mathbf{5}^{2+}$, which contains no solvent-based ligand.

Using the commercially available 2% $H_2{}^{18}O_2$ solutions increased the H_2O content significantly, so that CSI-MS measurements were not possible because of plugging of the spray needle by strong ice formation. Therefore, we performed experiments using $\mathbf{1}(ClO_4)_3$ obtained from bulk synthesis with labeled $H_2{}^{18}O_2$ and $H_2{}^{18}O$ (see the SI for details). CSI-MS experiments in CH_3CN at −40 °C on unlabeled samples showed peaks for $\mathbf{1}^{3+}$ at m/z 237.0711 and for $\{\mathbf{1}(ClO_4)\}^{2+}$ at m/z 405.0814 (Figure S19). Samples prepared with $H_2{}^{18}O_2$ (2% in $H_2{}^{16}O$) showed additional peaks at m/z 237.7384 and 406.0827 corresponding to the incorporation of one ^{18}O (Figure S20a−c). MS/MS experiments demonstrated that this ^{18}O was incorporated only in formate because, after formate release, only a μ-^{16}O species was present, whereas after release of the oxo bridge, both μ-$^{18}O^{16}OCH$ and μ-$^{16}O_2CH$ were detected (Figure S20d,e). Note that the ligand susan is monodeprotonated upon the release of formate and doubly deprotonated upon release of the oxo dianion. Thus, it can be concluded that stable dinuclear species exist with the highest overall charge of 3+. In summary, the reaction with $H_2{}^{18}O_2$ in the presence of excess $H_2{}^{16}O$ results in the formation of $\{Fe(\mu\text{-}^{16}O)(\mu\text{-}^{18}O^{16}OCH)Fe\}$ ($\mathbf{1b}^{3+}$) and $\{Fe(\mu\text{-}^{16}O)(\mu\text{-}^{16}O_2CH)Fe\}$ ($\mathbf{1d}^{3+}$; Figure 5, left).

Samples prepared with $H_2{}^{16}O_2$ in $H_2{}^{16}O$ dissolved in $H_2{}^{18}O$ (final $H_2{}^{18}O$:$H_2{}^{16}O$ = 26:1) provided in the addition to peaks with only ^{16}O at m/z 237.0720 and with the incorporation of one ^{18}O at m/z 237.7392 (Figure S21a) and also $\mathbf{1}^{3+}$ with two ^{18}O incorporated at m/z 238.4073 (Figure S21b; analogous results for $\{\mathbf{1}(ClO_4)\}^{2+}$ in Figure S21c), which accounts for the fact that oxygen from water was incorporated as an oxo atom in the high-valent oxidant **Y**. In the CSI-MS/MS experiments (Figure S21d), we detected the formato-bridged μ-$^{18}O^{16}OCH$ and μ-$^{16}O_2CH$ species (resulting from removal of an oxo bridge; Figure S21e), as well as the oxo-bridged μ-^{16}O and μ-^{18}O species (resulting from removal of a formate bridge; Figure S21f). Thus, the four differently labeled species $\mathbf{1d}^{3+}$, $\{Fe(\mu\text{-}^{18}O)(\mu\text{-}^{16}O_2CH)Fe\}$ ($\mathbf{1a}^{3+}$), $\{Fe(\mu\text{-}^{18}O)(\mu\text{-}^{18}O^{16}OCH)\}$ ($\mathbf{1c}^{3+}$), and $\{Fe(\mu\text{-}^{16}O)(\mu\text{-}^{16}O^{18}OCH)Fe\}$ ($\mathbf{1b}^{3+}$) were formed as the parent species.

These experiments clearly show that the μ-oxo atom, as well as one oxygen from peroxide (obtained after O−O bond splitting), is able to be transferred to CH_3OH and unequivocally demonstrate that the formate in $\mathbf{1}^{3+}$ originates from the oxidation of CH_3OH initiated by formation of the peroxo complex $\mathbf{5}^{2+}$. Moreover, ^{18}O incorporation in formate from the μ-^{18}O-bridged $\mathbf{5}^{2+}$ cannot be explained by this peroxo $\mathbf{5}^{2+}$ or corresponding hydroperoxo species as the active species. Thus, $\mathbf{5}^{2+}$ must rearrange into the active oxidant **Y**, which has two oxygen atoms that can be transferred onto the substrate: one originating from H_2O_2 and one from the oxo bridge. The latter suggests that the active oxidant **Y** is a high-valent species favoring the formation of a transient $Fe^{IV}Fe^{IV}$ intermediate.

In analogy to MMO,[11,12] the peroxo complex $\mathbf{5}^{2+}$ can convert to either a "closed" core intermediate, $[(susan)\{Fe^{IV}(\mu\text{-}O)_2Fe^{IV}\}]^{4+}$ ($\mathbf{6}^{4+}$), or an "open" core intermediate, $[(susan)\{Fe^{IV}(O)(\mu\text{-}O)Fe^{IV}(O)\}]^{2+}$ ($\mathbf{7b}^{2+}$; Figure 5). Considering the "closed" core structure, the use of $H_2{}^{18}O$ results via peroxo species $\mathbf{5a}^{2+}$ to the oxidant $\mathbf{6}^{4+}$ with one μ-^{18}O incorporated. The same species results by the use of $H_2{}^{18}O_2$ via peroxo species $\mathbf{5b}^{2+}$ after ^{18}O−^{18}O splitting. Both oxo bridges can be incorporated in formate, consistent with the observation of both μ-$^{16}O_2CH$ and μ-$^{16}O^{18}OCH$. In the $H_2{}^{18}O_2$-labeling experiment, the ratio of $H_2{}^{16}O/H_2{}^{18}O$ is 616:1, with 1 equiv of $H_2{}^{18}O$ resulting from splitting of the ^{18}O−^{18}O bond. The excess of $H_2{}^{16}O$ exchanges μ-^{18}O in $\mathbf{1a}^{3+}$, resulting in $\mathbf{1d}^{3+}$. In the $H_2{}^{18}O$-labeling experiment, there is still enough $H_2{}^{16}O$ present in solution, so that also some unlabeled $\mathbf{1d}^{3+}$ can be detected.

Considering an "open core" $\mathbf{7}^{2+}$, the reaction with $H_2{}^{18}O_2$ would generate $\mathbf{7b}^{2+}$, whereas the reaction with $H_2{}^{18}O$ would result in $[(susan)\{Fe^{IV}(^{16}O)(\mu\text{-}^{18}O)Fe^{IV}(^{16}O)\}]^{2+}$ ($\mathbf{7a}^{2+}$). Under the highly probable assumption that only the terminal oxo ligands can be incorporated into the formato bridge, one would expect the formation of only μ-$HC^{18}O^{16}O$ ($\mathbf{1b}^{3+}$) from the reaction with $H_2{}^{18}O_2$ and μ-$HC^{16}O_2$ ($\mathbf{1a}^{3+}$) from the reaction with $H_2{}^{18}O$. The formation of other observed isotopically labeled products through the "open core" pathway would require a scrambling between terminal and bridging oxo ligands.

■ SUMMARY AND CONCLUSIONS

We have carefully studied the catalytic oxidation of CH_3OH with H_2O_2 to HCHO, HCO_2H, and CO_2 by a dinuclear iron complex. The electrocatalytic oxidation of CH_3OH to CO_2 is the basis for the direct CH_3OH fuel cell.[42,43] The homogeneous catalytic oxidation of CH_3OH to HCHO has been established for copper(II) phenoxyl radical models of the enzyme galactose oxidase.[44−47] The application of homogeneous Fe catalysts for the oxidation of CH_3OH has rarely been reported. Lecomte and Bolm reported the combination of $[Fe(acac)_3]$ with H_2O_2 to oxidize CH_3OH to HCHO that is used in situ for an Aldol coupling.[48]

To the best of our knowledge, we have in detail investigated for the first time the homogeneous catalytic oxidation of CH_3OH by a high-valent diiron complex and obtained mechanistic insight into the nature of the active oxidant and the influence of the protonation state. The complex $\mathbf{4}^{2+}$ reacts with H_2O_2 to the peroxo complex $\mathbf{5}^{2+}$. Without protonation, exchange of the CH_3O^- ligands is slow, while its protonation accelerates exchange even at −80 °C. Furthermore, the protonation state affects the half-life of the peroxo intermediate: without protonation, the μ-peroxo intermediate converts slower to the active oxidant **Y** than in the protonated, presumably a μ-hydroperoxo, form.[26,28,41] The highly reactive oxidant **Y** initiates the oxidation of CH_3OH. ^{18}O-labeling

https://dx.doi.org/10.1021/acs.inorgchem.0c02698
Inorg. Chem. XXXX, XXX, XXX−XXX

experiments demonstrate that **Y** contains two distinguishable reactive oxygen atoms from its peroxo precursor: one from the μ-oxo bridge and one from the μ-peroxo bridge. This is in contrast to sMMO, where both oxygen atoms of the μ-peroxo bridge in **P** are reactive in **Q**.[10] The observed isotopic labeling can be explained with a "closed" $\{Fe^{IV}(\mu\text{-}O)_2Fe^{IV}\}$ core active species $\mathbf{6}^{4+}$, while its formulation as an "open" $\{Fe^{IV}(O)(\mu\text{-}O)Fe^{IV}(O)\}$ core $\mathbf{7}^{2+}$ requires a scrambling between terminal and bridging oxo ligands, which was formulated in a related system by Kodera et al.[21] In order to better distinguish between the "closed" or "open" core nature of oxidant **Y**, further studies are needed. We will vary the substitution pattern of the ligand susan, in analogy to the work with tpa-based ligands,[19−31] to stabilize, on the one hand, the μ-peroxo intermediate and, on the other hand, the high-valent oxidant **Y**.

■ ASSOCIATED CONTENT

Supporting Information

The Supporting Information is available free of charge at https://pubs.acs.org/doi/10.1021/acs.inorgchem.0c02698.

Experimental details on synthesis and catalysis, crystal structure determination, Mössbauer, UV−vis, and NMR spectra, and CSI-MS and CSI-MS/MS (PDF)

Accession Codes

CCDC 1986459 contains the supplementary crystallographic data for this paper. These data can be obtained free of charge via www.ccdc.cam.ac.uk/data_request/cif, or by emailing data_request@ccdc.cam.ac.uk, or by contacting The Cambridge Crystallographic Data Centre, 12 Union Road, Cambridge CB2 1EZ, UK; fax: +44 1223 336033.

■ AUTHOR INFORMATION

Corresponding Authors

Ivana Ivanović-Burmazović − *Department Chemie und Pharmazie, Friedrich-Alexander-Universität Erlangen-Nürnberg, Erlangen, Germany; Department Chemie, Ludwigs-Maximilians-Universität, 81377 München, Germany*; Email: Ivana.Ivanovic-Burmazovic@cup.uni-muenchen.de

Thorsten Glaser − *Fakultät für Chemie, Universität Bielefeld, D-33615 Bielefeld, Germany*; orcid.org/0000-0003-2056-7701; Email: thorsten.glaser@uni-bielefeld.de

Authors

Thomas Philipp Zimmermann − *Fakultät für Chemie, Universität Bielefeld, D-33615 Bielefeld, Germany*

Nicole Orth − *Department Chemie und Pharmazie, Friedrich-Alexander-Universität Erlangen-Nürnberg, Erlangen, Germany*

Sebastian Finke − *Fakultät für Chemie, Universität Bielefeld, D-33615 Bielefeld, Germany*

Thomas Limpke − *Fakultät für Chemie, Universität Bielefeld, D-33615 Bielefeld, Germany*

Anja Stammler − *Fakultät für Chemie, Universität Bielefeld, D-33615 Bielefeld, Germany*

Hartmut Bögge − *Fakultät für Chemie, Universität Bielefeld, D-33615 Bielefeld, Germany*

Stephan Walleck − *Fakultät für Chemie, Universität Bielefeld, D-33615 Bielefeld, Germany*

Complete contact information is available at: https://pubs.acs.org/10.1021/acs.inorgchem.0c02698

Author Contributions

†These authors contributed equally to this work.

Notes

The authors declare no competing financial interest.

■ ACKNOWLEDGMENTS

T.G. acknowledges the DFG and Bielefeld University of financial support. I.I.-B. thanks the DFG for support through Project IV 80/13-1.

■ REFERENCES

(1) Jasniewski, A. J.; Que, L. Dioxygen Activation by Nonheme Diiron Enzymes: Diverse Dioxygen Adducts, High-Valent Intermediates, and Related Model Complexes. *Chem. Rev.* **2018**, *118*, 2554−2592.

(2) Solomon, E. I.; Brunold, T. C.; Davis, M. I.; Kemsley, J. N.; Lee, S.-K.; Lehnert, N.; Neese, F.; Skulan, A. J.; Yang, Y.-S.; Zhou, J. Geometric and Electronic Structure/Function Correlations in Non-Heme Iron Enzymes. *Chem. Rev.* **2000**, *100*, 235−349.

(3) Ray, K.; Pfaff, F. F.; Wang, B.; Nam, W. Status of reactive non-heme metal-oxygen intermediates in chemical and enzymatic reactions. *J. Am. Chem. Soc.* **2014**, *136*, 13942−13958.

(4) Wallar, B. J.; Lipscomb, J. D. Dioxygen activation by enzymes containing binuclear non-heme iron clusters. *Chem. Rev.* **1996**, *96*, 2625−2657.

(5) Tinberg, C. E.; Lippard, S. J. Dioxygen activation in soluble methane monooxygenase. *Acc. Chem. Res.* **2011**, *44*, 280−288.

(6) Merkx, M.; Kopp, D. A.; Sazinsky, M. H.; Blazyk, J. L.; Müller, J.; Lippard, S. L. Dioxygen activation and methane hydroxylation by soluble methane monooxygenase: A tale of two irons and three proteins. *Angew. Chem., Int. Ed.* **2001**, *40*, 2782−2807.

(7) Komor, A. J.; Rivard, B. S.; Fan, R.; Guo, Y.; Que, L.; Lipscomb, J. D. Mechanism for Six-Electron Aryl-N-Oxygenation by the Non-Heme Diiron Enzyme CmlI. *J. Am. Chem. Soc.* **2016**, *138*, 7411−7421.

(8) Komor, A. J.; Rivard, B. S.; Fan, R.; Guo, Y.; Que, L.; Lipscomb, J. D. CmlI N-Oxygenase Catalyzes the Final Three Steps in Chloramphenicol Biosynthesis without Dissociation of Intermediates. *Biochemistry* **2017**, *56*, 4940−4950.

(9) Shu, L.; Nesheim, J. C.; Kauffmann, K.; Münck, E.; Lipscomb, J. D.; Que, L., Jr. An $Fe^{IV}{}_2O_2$ diamond core structure for the key intermediate Q of methane monooxygenase. *Science* **1997**, *275*, 515−518.

(10) Banerjee, R.; Proshlyakov, Y.; Lipscomb, J. D.; Proshlyakov, D. A. Structure of the key species in the enzymatic oxidation of methane to methanol. *Nature* **2015**, *518*, 431−434.

(11) Castillo, R. G.; Banerjee, R.; Allpress, C. J.; Rohde, G. T.; Bill, E.; Que, L.; Lipscomb, J. D.; DeBeer, S. High-Energy-Resolution Fluorescence-Detected X-ray Absorption of the Q Intermediate of Soluble Methane Monooxygenase. *J. Am. Chem. Soc.* **2017**, *139*, 18024−18033.

(12) Cutsail, G. E.; Banerjee, R.; Zhou, A.; Que, L.; Lipscomb, J. D.; DeBeer, S. High-Resolution Extended X-ray Absorption Fine Structure Analysis Provides Evidence for a Longer Fe···Fe Distance in the Q Intermediate of Methane Monooxygenase. *J. Am. Chem. Soc.* **2018**, *140*, 16807−16820.

(13) Jiang, Y.; Wilkins, P. C.; Dalton, H. Activation of the hydroxylase of sMMO from Methylococcus capsulatus (Bath) by hydrogen peroxide. *Biochim. Biophys. Acta, Protein Struct. Mol. Enzymol.* **1993**, *1163*, 105−112.

(14) Andersson, K. K., Froland, W. A., Lee, S. K.; Lipscomb, J. D. *New J. Chem.* **1991**.

(15) Zhang, X.; Furutachi, H.; Fujinami, S.; Nagatomo, S.; Maeda, Y.; Watanabe, Y.; Kitagawa, T.; Suzuki, M. Structural and spectroscopic characterization of (μ-hydroxo or μ-oxo)(μ-peroxo)-diiron(III) complexes: models for peroxo intermediates of non-heme diiron proteins. *J. Am. Chem. Soc.* **2005**, *127*, 826−827.

(16) Ookubo, T.; Sugimoto, H.; Nagayama, T.; Masuda, H.; Sato, T.; Tanaka, K.; Maeda, Y.; Ōkawa, H.; Hayashi, Y.; Uehara, A.; Suzuki, M. cis -μ-1,2-Peroxo Diiron Complex: Structure and Reversible Oxygenation. *J. Am. Chem. Soc.* **1996**, *118*, 701−702.

(17) Kim, K.; Lippard, S. J. Structure and Mössbauer Spectrum of a (μ-1,2-Peroxo)bis(μ-carboxylato)diiron(III) Model for the Peroxo Intermediate in the Methane Monooxygenase Hydroxylase Reaction Cycle. *J. Am. Chem. Soc.* **1996**, *118*, 4914−4915.
(18) Dong, Y.; Yan, S.; Young, V. G.; Que, L. Crystal Structure Analysis of a Synthetic Non-Heme Diiron−O_2 Adduct: Insight into the Mechanism of Oxygen Activation. *Angew. Chem., Int. Ed. Engl.* **1996**, *35*, 618−620.
(19) Dong, Y.; Zang, Y.; Shu, L.; Wilkinson, E. C.; Que Jr, L.; Kauffmann, K.; Münck, E. Models for Nonheme Diiron Enzymes. Assembly of a High-Valent $Fe_2(\mu\text{-}O)_2$ Diamond Core from Its Peroxo Precursor. *J. Am. Chem. Soc.* **1997**, *119*, 12683−12684.
(20) Kodera, M.; Taniike, Y.; Itoh, M.; Tanahashi, Y.; Shimakoshi, H.; Kano, K.; Hirota, S.; Iijima, S.; Ohba, M.; Okawa, H. Synthesis, Characterization, and Activation of Thermally Stable μ-1,2-Peroxodiiron(III) Complex. *Inorg. Chem.* **2001**, *40*, 4821−4822.
(21) Kodera, M.; Itoh, M.; Kano, K.; Funabiki, T.; Reglier, M. A diiron center stabilized by a bis-TPA ligand as a model of soluble methane monooxygenase: predominant alkene epoxidation with H_2O_2. *Angew. Chem., Int. Ed.* **2005**, *44*, 7104−7106.
(22) Fiedler, A. T.; Shan, X.; Mehn, M. P.; Kaizer, J.; Torelli, S.; Frisch, J. R.; Kodera, M.; Que, L., Jr. Spectroscopic and computational studies of (μ-oxo)(μ-1,2-peroxo)diiron(III) complexes of relevance to nonheme diiron oxygenase intermediates. *J. Phys. Chem. A* **2008**, *112*, 13037−13044.
(23) Kryatov, S. V.; Rybak-Akimova, E. V. A kinetic study of the formation of a model high-valent diiron non-heme complex, [$Fe^{III}Fe^{IV}$(μ-O)2(tpa)2]3+ (tpa = tris(2-pyridylmethyl)amine), by cryogenic stopped-flow techniques †. *J. Chem. Soc., Dalton Trans.* **1999**, 3335−3336.
(24) Dong, Y.; Fujii, H.; Hendrich, M. P.; Leising, R. A.; Pan, G.; Randall, C. R.; Wilkinson, E. C.; Zang, Y.; Que, L., Jr. A High-Valent Nonheme Iron Intermediate. Structure and Properties of [$Fe_2(\mu\text{-}O)_2$(5-Me-TPA)$_2$](ClO_4)$_3$. *J. Am. Chem. Soc.* **1995**, *117*, 2778−2792.
(25) Dong, Y.; Que Jr, L.; Kauffmann, K.; Muenck, E. An Exchange-Coupled Complex with Localized High-Spin Fe^{IV} and Fe^{III} Sites of Relevance to Cluster X of Escherichia coli Ribonucleotide Reductase. *J. Am. Chem. Soc.* **1995**, *117*, 11377−11378.
(26) Xue, G.; Fiedler, A. T.; Martinho, M.; Munck, E.; Que, L., Jr. Insights into the P-to-Q conversion in the catalytic cycle of methane monooxygenase from a synthetic model system. *Proc. Natl. Acad. Sci. U. S. A.* **2008**, *105*, 20615−20620.
(27) Xue, G.; De Hont, R.; Münck, E.; Que, L., Jr. Million-fold activation of the [$Fe_2(\mu\text{-}O)_2$] diamond core for C-H bond cleavage. *Nat. Chem.* **2010**, *2*, 400−405.
(28) Do, L. H.; Xue, G.; Que, L., Jr.; Lippard, S. J. Evaluating the identity and diiron core transformations of a (μ-oxo)diiron(III) complex supported by electron-rich tris(pyridyl-2-methyl)amine ligands. *Inorg. Chem.* **2012**, *51*, 2393−2402.
(29) Stoian, S. A.; Xue, G.; Bominaar, E. L.; Que, L.; Münck, E. Spectroscopic and theoretical investigation of a complex with an O = Fe(IV)-O-Fe(IV)═O core related to methane monooxygenase intermediate Q. *J. Am. Chem. Soc.* **2014**, *136*, 1545−1558.
(30) Kodera, M.; Kawahara, Y.; Hitomi, Y.; Nomura, T.; Ogura, T.; Kobayashi, Y. Reversible O-O bond scission of peroxodiiron(III) to high-spin oxodiiron(IV) in dioxygen activation of a diiron center with a bis-tpa dinucleating ligand as a soluble methane monooxygenase model. *J. Am. Chem. Soc.* **2012**, *134*, 13236−13239.
(31) Kodera, M.; Ishiga, S.; Tsuji, T.; Sakurai, K.; Hitomi, Y.; Shiota, Y.; Sajith, P. K.; Yoshizawa, K.; Mieda, K.; Ogura, T. Formation and High Reactivity of the anti-Dioxo Form of High-Spin μ-Oxodioxodiiron(IV) as the Active Species That Cleaves Strong C-H Bonds. *Chem. - Eur. J.* **2016**, *22*, 5924−5936.
(32) Strautmann, J. B. H.; Walleck, S.; Bögge, H.; Stammler, A.; Glaser, T. A tailor-made ligand to mimic the active site of diiron enzymes: an air-oxidized high-valent Fe^{III} h.s.(μ-O)$_2Fe^{IV}$ h.s. species. *Chem. Commun.* **2011**, *47*, 695−697.
(33) Strautmann, J. B. H.; Dammers, S.; Limpke, T.; Parthier, J.; Zimmermann, T. P.; Walleck, S.; Heinze-Brückner, G.; Stammler, A.; Bögge, H.; Glaser, T. Design and synthesis of a dinucleating ligand system with varying terminal donor functions that provides no bridging donor and its application to the synthesis of a series of Fe^{III}-μ-O-Fe^{III} complexes. *Dalton Trans.* **2016**, *45*, 3340−3361.
(34) Glaser, T. A dinucleating ligand system with varying terminal donor functions but without bridging donor functions: Design, synthesis, and applications for diiron complexes. *Coord. Chem. Rev.* **2019**, *380*, 353−377.
(35) Zimmermann, T. P.; Limpke, T.; Stammler, A.; Bögge, H.; Walleck, S.; Glaser, T. Reversible Carboxylate Shift in a μ-Oxo Diferric Complex in Solution by Acid-/Base-Addition. *Inorg. Chem.* **2018**, *57*, 5400−5405.
(36) Norman, R. E.; Leising, R. A.; Yan, S.; Que, L. Unexpected assembly of a (μ-oxo)(μ-formato)diiron(III) complex from an aerobic methanolic solution of Fe(III) and the TPA ligand. *Inorg. Chim. Acta* **1998**, *273*, 393−396.
(37) Zimmermann, T. P.; Limpke, T.; Orth, N.; Franke, A.; Stammler, A.; Bögge, H.; Walleck, S.; Ivanovic-Burmazovic, I.; Glaser, T. Two Unsupported Terminal Hydroxo Ligands in a μ-Oxo-Bridged Ferric Dimer: Protonation and Kinetic Lability Studies. *Inorg. Chem.* **2018**, *57*, 10457−10468.
(38) Okuno, T.; Ito, S.; Ohba, S.; Nishida, Y. μ-Oxo bridged diiron(III) complexes and hydrogen peroxide: oxygenation and catalase-like activities. *J. Chem. Soc., Dalton Trans.* **1997**, 3547−3551.
(39) Ménage, S.; Vincent, J. M.; Lambeaux, C.; Fontecave, M. μ-Oxo-bridged diiron(III) complexes and H_2O_2: monooxygenase- and catalase-like activities. *J. Chem. Soc., Dalton Trans.* **1994**, *38*, 2081−2084.
(40) Zimmermann, T. P.; Limpke, T.; Stammler, A.; Bögge, H.; Walleck, S.; Glaser, T. Variation of the Molecular and Electronic Structures of μ-Oxo Diferric Complexes with the Bridging Motive. *Z. Anorg. Allg. Chem.* **2018**, *644*, 683−691.
(41) Park, K.; Li, N.; Kwak, Y.; Srnec, M.; Bell, C. B.; Liu, L. V.; Wong, S. D.; Yoda, Y.; Kitao, S.; Seto, M.; Hu, M.; Zhao, J.; Krebs, C.; Bollinger, J. M.; Solomon, E. I. Peroxide Activation for Electrophilic Reactivity by the Binuclear Non-heme Iron Enzyme AurF. *J. Am. Chem. Soc.* **2017**, *139*, 7062−7070.
(42) Hamnett, A. Mechanism and electrocatalysis in the direct methanol fuel cell. *Catal. Today* **1997**, *38*, 445−457.
(43) Bianchini, C.; Shen, P. K. Palladium-based electrocatalysts for alcohol oxidation in half cells and in direct alcohol fuel cells. *Chem. Rev.* **2009**, *109*, 4183−4206.
(44) Chaudhuri, P.; Hess, M.; Müller, J.; Hildenbrand, K.; Bill, E.; Weyhermüller, T.; Wieghardt, K. Aerobic Oxidation of Primary Alcohols (Including Methanol) by Copper(II)− and Zinc(II)−Phenoxyl Radical Catalysts. *J. Am. Chem. Soc.* **1999**, *121*, 9599−9610.
(45) Chaudhuri, P.; Hess, M.; Weyhermüller, T.; Wieghardt, K. Aerobic Oxidation of Primary Alcohols by a New Mononuclear CuII-Radical Catalyst. *Angew. Chem., Int. Ed.* **1999**, *38*, 1095−1098.
(46) Solomon, E. I.; Heppner, D. E.; Johnston, E. M.; Ginsbach, J. W.; Cirera, J.; Qayyum, M.; Kieber-Emmons, M. T.; Kjaergaard, C. H.; Hadt, R. G.; Tian, L. Copper active sites in biology. *Chem. Rev.* **2014**, *114*, 3659−3853.
(47) Elwell, C. E.; Gagnon, N. L.; Neisen, B. D.; Dhar, D.; Spaeth, A. D.; Yee, G. M.; Tolman, W. B. Copper-Oxygen Complexes Revisited: Structures, Spectroscopy, and Reactivity. *Chem. Rev.* **2017**, *117*, 2059−2107.
(48) Lecomte, V.; Bolm, C. Iron(III)-Catalyzed Tandem Sequential Methanol Oxidation/Aldol Coupling. *Adv. Synth. Catal.* **2005**, *347*, 1666−1672.

https://dx.doi.org/10.1021/acs.inorgchem.0c02698
Inorg. Chem. XXXX, XXX, XXX−XXX